

DEPARTMENT OF MANAGEMENT AND ENGINEERING

Modelling of failure

Master Thesis carried out at Division of Solid Mechanics
Linköpings University
March 2008

Oscar Björklund

LIU-IEI-TEK-A--08/00381--SE



Linköping University
INSTITUTE OF TECHNOLOGY

Institute of Technology, Dept. of Management and Engineering,
SE-581 83 Linköping, Sweden

Framläggningsdatum

Presentation date

2008-03-10

Publiceringsdatum

Publication date

2008-03-19

Avdelning, institution

Division, department

Division of Solid Mechanics

Dept. of Management and Engineering

SE-581 83 LINKÖPING

**Linköping University**
INSTITUTE OF TECHNOLOGY**Språk**

Language

Svenska/Swedish

X Engelska/English

Rapporttyp

Report category

Licentiatavhandling

X Examensarbete

C-uppsats

D-uppsats

Övrig rapport

ISBN:**ISRN:** LIU-IEI-TEK-A--08/00381--SE**Serietitel:**

Title of series

Serienummer/ISSN:

Number of series

URL för elektronisk version

URL for electronic version

<http://urn.kb.se/resolve?urn=urn:nbn:se:liu:diva-11466>**Titel**

Modelling of Failure

Title

Författare

Oscar Björklund

Author

Sammanfattning

Abstract

This report is a review of some failure models today used for determine failure in thin sheets of high strength steels. Focus has been given on phenomenological models and only some simple simulations have been carried out. The phenomenological models that have been summarized here are of four different categories, namely stress based, strain based, combined stress and strain based and damaged models. However, the simulations have only been preformed for some of the models.

Nyckelord:

Keyword

failure modelling, phenomelological, Cockcroft-Latham, Bressan-Williams, Gurson, Johnson-Cook
Wilkins, damage, LS-DYNA

Abstract

This report is a review of some failure models today used for determine failure in thin sheets of high strength steels. Focus has been given on phenomenological models and only some simple simulations have been carried out. The phenomenological models that have been summarized here are of four different categories, namely stress based, strain based, combined stress and strain based and damaged models. However, the simulations have only been preformed for some of the models.

Preface

The work presented here is the master thesis performed at the Division of Solid Mechanics at Linköpings University. The work is a first part of a literature study in the project FAIL which concerns failure in thin, high strength steel sheets.

A special thanks should be given to my supervisor Prof. Larsgunnar Nilsson and my co-supervisor Assoc. prof. Kjell Simonsson for all the help during the thesis. I would also like to thank all Ph.D. students and other diploma workers at the division for all their support.

A great appreciation should also be given to my family and friends for all their support during the years.

Linköping in March 2008
Oscar Björklund

Notation

Symbol	Meaning
E	Young modulus of elasticity
T	Temperature
\mathbf{A}	Transformation matrix
$\mathbf{e}_1, \mathbf{e}_2, \mathbf{e}_3$	Base vectors
Ω_0	Reference configuration
Ω	Current configuration
\mathbf{u}	Displacement vector
\mathbf{v}	Velocity vector
\mathbf{a}	Acceleration vector
\mathbf{F}	Deformation gradient tensor
\mathbf{R}	Rotation tensor
\mathbf{U}	Right stretch tensor
\mathbf{V}	Left stretch tensor
\mathbf{C}	Green deformation tensor
\mathbf{E}	Lagrange deformation tensor
\mathbf{L}	Velocity gradient tensor
\mathbf{D}	Rate of deformation tensor
\mathbf{W}	Spin tensor
ρ	Density
\mathbf{b}	Body forces
\mathbf{t}	Traction vector
e	Specific internal energy
\mathbf{q}	Heat flow
r	Inside generated heat
$\boldsymbol{\sigma}$	Cauchy stress tensor
σ_∞	Nominal stress
$\sigma_1, \sigma_2, \sigma_3$	Principal stresses
σ_m	Average normal stress
σ_{vM}	von Mises equivalent stress
σ_c	Maximum compression stress
σ_t	Maximum tension stress
σ_F	Fracture stress
σ_Y	Yielding stress
$\bar{\sigma}$	Equivalent stress
τ_c	Critical shear stress

Symbol	Meaning
$\varepsilon_1, \varepsilon_2, \varepsilon_3$	Principal strains
ε_f	Fracture strain
$\bar{\varepsilon}$	Equivalent strain
a	Crack length
G_C	Critical elastic energy release rate
K_{IC}	Fracture toughness
W	Elastic strain energy density
J	Rice integral
x_1, x_2, x_3	Coordinates
D	Damage variable
\vec{n}	Normal vector

Contents

1	Introduction	1
2	Continuum Mechanics	3
2.1	Constitutive relations	3
2.2	Tensor transformation	3
2.3	Kinematics	5
2.4	Conservation equations	8
3	Physical mechanisms of fracture	11
4	Fracture mechanics	13
5	Damage mechanics	15
6	Phenomeologic failure models	17
6.1	Stress dependent failure criteria	17
6.1.1	Maximum principle stress criterion	17
6.1.2	Tresca's and von Mises' failure criteria	18
6.1.3	Mohr's failure criterion	20
6.2	Strain dependent failure criteria	21
6.2.1	Maximum principle strain criterion	21
6.2.2	Constant equivalent strains criterion	21
6.2.3	Forming Limit Diagram	22
6.3	Cockcroft-Latham	23
6.4	Shear instability	24
6.5	Damage models	26
6.5.1	Gurson	27
6.5.2	Johnson-Cook	29
6.5.3	Wilkins	30
7	Plane strain test sample	31
8	Conclusions and discussion	43

1 Introduction

The automobile industry is more and more using computer simulations in the product development process in particular concerning passive safety. The main reasons for this are a reduced time and cost but also to be able to determine, at an early design state, if the car is safe from a crash point of view. The phenomenological models used today have a good agreement to reality as long as no failure occurs in a component. In physical testings of, e.g., frontal collisions, failures sometimes occur which not have been predicted in the simulations. The same is true for side impact tests, where failure sometimes occurs in the B-pillar which not were predicted by the simulations. As a result of the poor agreement between simulations and real crash tests, the project FAIL was initiated. The FAIL project is a collaboration project between SAAB Automobile, SSAB Tunnpååt, Outokumpu Stainless and Linköping University. The goal of the project is to evaluate and develop more accurate and effective phenomenological models for failure prediction in thin, high strength steel sheets used in a car body structure. As a first step in this project a literature review has been carried out.

2 Continuum Mechanics

From a physical point of view all materials are built up by atoms, which in turn consist of protons, neutrons and electrons. The strength of a material is due to the bindings between atoms. However, the bodies of interest are very large compared to the size of the atoms. From a practical point of view it is therefore in most analyses necessary to approximate the body as being continuous or at least partly continuous. The continuum mechanics are describing the phenomena of a continuous body, see Mase and Mase [1], Spencer [2] and Belytschko [3]. In this report all coordinate systems that are used are Cartesian unless otherwise is stated.

2.1 Constitutive relations

The constitutive equations are relating the stresses to strains in the material. One of the most commonly known constitutive equation is the Hooke's law which is representing the behaviour of a linear elastic material. For the three-dimensional case the law is

$$\begin{aligned}\boldsymbol{\sigma} &= \mathbf{C} : \boldsymbol{\varepsilon} \\ \sigma_{ij} &= C_{ijkl}\varepsilon_{kl}\end{aligned}\tag{1}$$

where \mathbf{C} is the fourth order material stiffness tensor. There are more advanced constitutive relations describing how the stress depends on other mechanical properties, and for a general case the stress can be expressed as a function of the type

$$\sigma = f(\varepsilon, \dot{\varepsilon}, T, \dots)\tag{2}$$

2.2 Tensor transformation

Most entities in continuum mechanics are represented as tensors, e.g. the velocity which is a first order tensor and the stress which is a second order tensor. This means that their components will change according to specific rules when changing from one coordinate system to another. The equations that transforms the components from one coordinate system to another are called the transformation equations. If one is trying to express the base

vectors \mathbf{e}_1 , \mathbf{e}_2 and \mathbf{e}_3 in the new coordinate system with base vectors $\tilde{\mathbf{e}}_1$, $\tilde{\mathbf{e}}_2$ and $\tilde{\mathbf{e}}_3$ this could be done by the matrix \mathbf{A} according to

$$\begin{pmatrix} \tilde{\mathbf{e}}_1 \\ \tilde{\mathbf{e}}_2 \\ \tilde{\mathbf{e}}_3 \end{pmatrix} = \begin{bmatrix} A_{11} & A_{12} & A_{13} \\ A_{21} & A_{22} & A_{23} \\ A_{31} & A_{32} & A_{33} \end{bmatrix} \begin{pmatrix} \mathbf{e}_1 \\ \mathbf{e}_2 \\ \mathbf{e}_3 \end{pmatrix} \quad (3)$$

$$\tilde{\mathbf{e}} = \mathbf{A}\mathbf{e} \quad \text{and} \quad \mathbf{e} = \mathbf{A}^T\tilde{\mathbf{e}} \quad (4)$$

The components of a first order tensor is transformed according to Equation (5) and a second one according to Equation (6), where $\tilde{\mathbf{v}}$ denotes the components of the velocity tensor in the coordinate system with the base vectors $\tilde{\mathbf{e}}_1$, $\tilde{\mathbf{e}}_2$ and $\tilde{\mathbf{e}}_3$. \mathbf{v} denotes the component of the velocity tensor represented in the coordinate system with the base vectors \mathbf{e}_1 , \mathbf{e}_2 and \mathbf{e}_3 . $\tilde{\boldsymbol{\sigma}}$ and $\boldsymbol{\sigma}$ are the components obtained in a similar way.

$$\tilde{\mathbf{v}} = \mathbf{A}\mathbf{v} \quad (5)$$

$$\tilde{\boldsymbol{\sigma}} = \mathbf{A}\boldsymbol{\sigma}\mathbf{A}^T \quad (6)$$

In some applications, when operating with anisotropic materials, it may be a good idea to express the tensor in a coordinate system that rotates with the material. In that case the corotated stress can be expressed as

$$\hat{\boldsymbol{\sigma}} = \mathbf{R}\boldsymbol{\sigma}\mathbf{R}^T \quad (7)$$

The difference between \mathbf{A} and \mathbf{R} is that \mathbf{R} only represents a rotation of the axes while the \mathbf{A} can also contain a scaling.

2.3 Kinematics

Kinematics is the study of motion, without consideration of the mass or forces that causes it. To be able to describe any motion it is necessary to define a coordinate system, in this case a fixed Cartesian coordinate system, defined by an origin O and base vectors \mathbf{e}_1 , \mathbf{e}_2 and \mathbf{e}_3 . Then at time $t = 0$ a reference configuration is defined, named Ω_0 . At time t the same body is at another place in space, which is denoted Ω and referred to as the current configuration. In some applications even an intermediate configuration is needed. Then considering a material point P_0 in the reference configuration a vector from O to P_0 is defined as \mathbf{X} ($\overrightarrow{OP_0} = \mathbf{X}$). A moment later the same point is at P in Ω with the associated vector \mathbf{x} going from O to P . The Lagrangian displacement vector \mathbf{u} can then be defined as

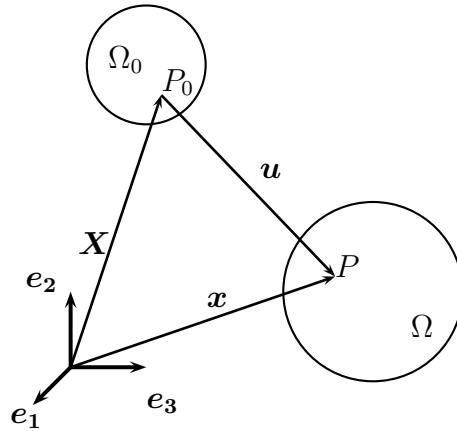


Figure 1: *Positions of a material particle in the reference and the current configurations*

$$\mathbf{u} = \mathbf{x} - \mathbf{X} \quad (8)$$

The deformation gradient \mathbf{F} and its inverse \mathbf{F}^{-1} are defined as

$$F_{ij} = \frac{\partial x_i}{\partial X_j} \quad F_{ij}^{-1} = \frac{\partial X_i}{\partial x_j} \quad (9)$$

Furthermore, it can be shown that the deformation gradient can be split into one orthogonal rotation tensor \mathbf{R} and one positive definite symmetric, so called right stretch tensor \mathbf{U} or one left stretch tensor \mathbf{V} in the following way

$$\mathbf{F} = \mathbf{R} \cdot \mathbf{U} = \mathbf{V} \cdot \mathbf{R} \quad (10)$$

The deformation gradient can then be seen as a first stretching of the body and then rotating it like in the upper part of Figure 2 or as in the lower part of this figure where the body is first rotated and then stretched.

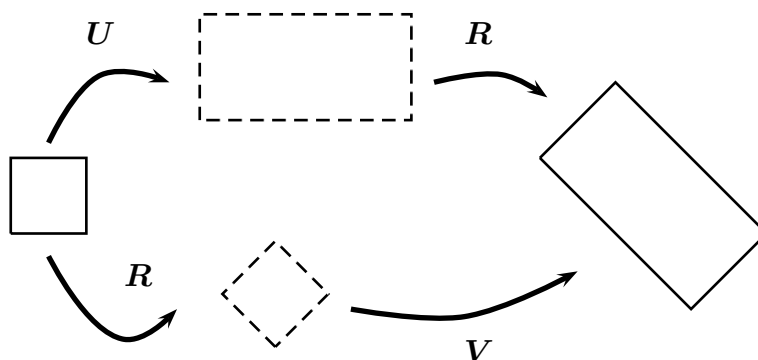


Figure 2: *Polar decomposition. The deformation can be seen as in the upper picture where the body is first stretched and then rotated, or as in the lower picture where it is first rotated and then stretched*

With this deformation tensor it is possible to construct other deformation tensors such as the Green deformation tensor in Equation (11) or the Lagrangian finite strain tensor in Equation (12)

$$\mathbf{C} = \mathbf{F}^T \cdot \mathbf{F} \quad (11)$$

$$\mathbf{E} = \frac{1}{2} (\mathbf{F}^T \cdot \mathbf{F} - \mathbf{I}) = \frac{1}{2} (\mathbf{C} - \mathbf{I}) \quad (12)$$

When considering small strains it is possible to split the total strain into one elastic and one plastic part according to

$$\boldsymbol{\varepsilon} = \boldsymbol{\varepsilon}_e + \boldsymbol{\varepsilon}_p \quad (13)$$

where the index e and p denoted elastic or plastic strain. In case of large deformations the deformation gradient can be split into one elastic part and one plastic part in a multiplicative way

$$\mathbf{F} = \mathbf{F}^e \mathbf{F}^p \quad (14)$$

Figure 3 describes the deformation from the reference configuration (Ω_0) to the current configuration (Ω). It can be seen as a plastic deformation \mathbf{F}^p to an intermediate configuration and then an elastic deformation \mathbf{F}^e to the current configuration.

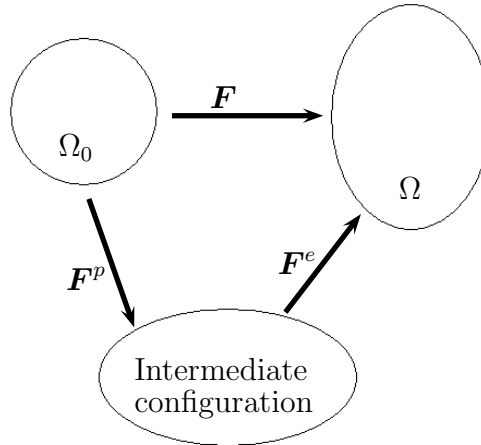


Figure 3: *Split of the deformation gradient into one elastic and one plastic part*

The Lagrangian velocity field \mathbf{v} is defined as $v_i = \frac{\partial u_i}{\partial t}$ since \mathbf{X} is independent of time. The spatial velocity gradient is defined as

$$L_{ij} = \frac{\partial v_i}{\partial x_j} \quad (15)$$

The velocity gradient can be split into one symmetric tensor \mathbf{D} and one skew-symmetric tensor \mathbf{W} according to

$$L_{ij} = \frac{1}{2} \left(\frac{\partial v_i}{\partial x_j} + \frac{\partial v_j}{\partial x_i} \right) + \frac{1}{2} \left(\frac{\partial v_i}{\partial x_j} - \frac{\partial v_j}{\partial x_i} \right) = D_{ij} + W_{ij} \quad (16)$$

where \mathbf{D} is called the rate of deformation tensor and \mathbf{W} is called the spin tensor.

2.4 Conservation equations

In continuum mechanics some basic equations exist. First there are four conservation laws. The first one, the conservation of mass, requires that the mass of any material domain remains constant. If no material flows through the boundaries of the material

$$\frac{d}{dt} \int_{\Omega} \rho dV = 0 \quad (17)$$

The second law is the conservation of linear momentum, which can be expressed as

$$\frac{d}{dt} \int_{\Omega} \rho \mathbf{v} dV = \int_{\Omega} \rho \mathbf{b} dV + \int_{\partial\Omega} \mathbf{t} dS \quad (18)$$

where \mathbf{b} is body forces and \mathbf{t} is the surface traction ($t_i = \sigma_{ij}n_j$). By using Reynold's transport theorem, Cauchy's relation and the Gauss's theorem, one can transform all integrals into volume integrals over the domain Ω and since this should be valid regardless of the choice of such a domain, one obtain the equation of motion

$$\frac{\partial \sigma_{ij}}{\partial x_j} + \rho b_i = \rho a_i \quad (19)$$

where σ_{ij} is the Cauchy stress tensor, ρ is the density, b_i is body forces and a_i is the acceleration of the material point. The third law is the conservation of angular momentum which implies that the Cauchy stress tensor is symmetric.

$$\boldsymbol{\sigma} = \boldsymbol{\sigma}^T \quad \text{or} \quad \sigma_{ij} = \sigma_{ji} \quad (20)$$

The last conservation law is the conservation of energy, which is also known as the first law of thermodynamics. The law implies that the rate of change of total energy is equal to the work done by body forces and surface tractions and supplied heat per time unit.

$$\begin{aligned} & \frac{d}{dt} \left(\int_{\Omega} \rho e dV + \frac{1}{2} \int_{\Omega} \rho \mathbf{v} \cdot \mathbf{v} dV \right) = \\ & = \int_{\Omega} \rho \mathbf{b} \cdot \mathbf{v} dV + \int_{\partial\Omega} \mathbf{t} \cdot \mathbf{v} dS + \int_{\Omega} r dV - \int_{\partial\Omega} \mathbf{q} \cdot \mathbf{n} dS \end{aligned} \quad (21)$$

where e is the specific internal energy per unit mass and \mathbf{q} is the heat flux. The parameter r is the heat generated inside the body. From this expression we can obtain

$$\rho \dot{e} = \boldsymbol{\sigma} : \mathbf{D} + r - \text{div } \mathbf{q} \quad (22)$$

where \dot{e} is the time derivative of the specific internal energy and \mathbf{D} is the rate of deformation tensor defined in the previous section.

3 Physical mechanisms of fracture

To be able to formulate the hypothesis upon which macroscopic phenomenological fracture models are based, it is necessary to understand the basic physical mechanism, that are causing the failure in the material. More detailed information is given in, e.g. Askeland [4], Hertzberg [5], Dieter [6] and Lemaitre and Chaboche [7]

Elastic or plastic deformations, which take place on a atomic or crystalline levels, do not destroys the order of the material, while fracture on the other hand cause discontinuities within the material. This discontinuities cause stress concentrations which will increase the 'rate' of the fracture. There is two main types of fracture, namely brittle and ductile.

Brittle fracture is the fracture of interatomic bounds without noticeable plastic deformation. This fracture occur when the local strain energy becomes larger then the energy necessary to pull the atom layers apart. Brittle fracture occurs mainly in high-strength metals with poor ductility and toughness. However, even metals that have normal ductility may fail in a brittle way at low temperatures, in thick sections or at high strain rates, the latter might be the case in vehicle crash situations. The surface of a brittle fracture is characterized by its flat appearers and it is also perpendicular to the applied load.

Ductile fracture, on the other hand, is caused by instability which is a result from very large plastic deformations occuring in the surrounding of crystalline defects. The deformation in ductile fracture can be both large and small depending on the density of the defects. The fracture surface of the ductile fracture is characterized by the shear lips that are present, see Figure 4, which leads to the form of a cup and a cone for the two surfaces in a microscope. It is also often possible to see the dimples that are caused by the micro-voids.

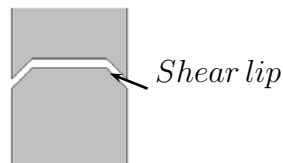


Figure 4: *Shear lips appearance in a ductile fracture zone*

4 Fracture mechanics

The concept of fracture mechanics is the study of cracks in solid materials. It goes back to the beginning of the 20th century when Griffith introduced his energy method, which for a simple case of a thin rectangular plate with a crack perpendicular to the load becomes

$$\frac{\sigma_{\infty}^2 \pi a}{E} > G_C \quad (23)$$

where σ_{∞} is the nominal stress far away from the crack tip, a is the crack length, E is Young's modulus of elasticity and G_C is the critical elastic energy release rate.

Even though the Griffith's concept was introduced earlier it was not until the World War II, when Irwin and coworkers started to work with fracture mechanics, that it became used in industrial applications. Irwin and coworkers used a stress based model instead of the energy based Griffith model. In their model they introduced a new material property, fracture toughness (K_{IC}) which has the unit $N m^{3/2}$ or $Pa m^{1/2}$. For the same case as above the Irwin model becomes

$$\sigma_{\infty} \sqrt{\pi a} \leq K_{IC} \quad (24)$$

The fracture models of Griffith and Irwin are only valid for linear elastic materials. Rice however introduced a more advanced method to solve the fracture problems where plastic deformations are present. He considered the J integral and said that when this parameter reach a certain value fracture occurs. The J , or Rice integral is, defined as

$$J = \int_{\Gamma} W dx_2 - \int_{\Gamma} \left(\mathbf{t} \frac{\partial \mathbf{u}}{\partial x_1} \right) ds \quad (25)$$

where W is the elastic strain energy density, \mathbf{t} is the traction vector acting on the contour around the crack, \mathbf{u} is the displacement vector and ds is an increment of the contour path, see Figure 5. Note that all the above models are valid for two-dimensional cases.

For more information on fracture mechanics, see Hertzberg [5], Dieter [6], Lemaitre and Chaboche [7] and Dahlberg and Ekberg [8].

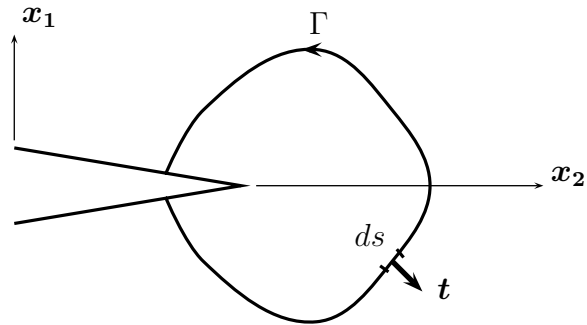


Figure 5: *Sketch of the Γ contour drawn around a crack tip to define the J (Rice) integral*

In a Finite Element analysis of a crash simulation the concept of fracture mechanics will be too expensive considering computing time and therefore it is not further investigated in this study. In this rapport only stress, strain and damage mechanics models to predict failure are studied.

5 Damage mechanics

The basic idea of damage mechanics is to translate the underlying microscopical failure phenomena to a macroscopical description that can be used in a phenomenological model. In all cases, discussed in this report, the models are considering one or more parameters and when these parameters reaches a critical value failure is expected.

Macroscopical fracture has been studied for a very long time. Even as early as in the beginning of 16th century, Leonardo da Vinci was explaining the fracture in terms of mechanical variables. He established that the load an iron wire could carry strongly depends on the length of the wire as a consequence of the amount of voids in the material; the longer wire the more voids which lead to a lower load carrying capacity.

A number of failure criteria in terms of stresses and strains to characterize the fracture of a body have been proposed, e.g., by Coulumb, Rankine, Tresca, von Mises et al.. These simple failure models only consider the stress or strain, while more complex models such as the Cockroft-Latham model also depend on the loading history.

In recent years models concerning different type of damages have been studied, e.g. by Gurson, Johnsson-Cook and Wilkins, which all are trying to describe the new formation, growth and coalescence of micro-voids in terms of mechanical properties. In this case more properties are needed, for instance the strain rate, stress triaxiality and temperature are included in the Johnsson-Cook model. Most crash simulations of today do not use damage models due to a lack of information on which damage models that under given conditions give reliable predictions, and how the damage parameters should be determined. The report by Feucht et al. [9] shows the difficulties and benefits of such models.

6 Phenomelogic failure models

The phenomelogical models describe the failure in the material in terms of mechanical variables such as stress, strain, temperature, strain rate etc. In all models presented in this work the failure model is a function which depends of these variables and if the functions reaches a critical value, failure is expected in the material. The report by Wierzbicki et al. [10] contains information on calibration of some of the models presented in this report. The models that are presented in this report can be classified in four different groupes as models dependent on stress, strain or a combination of stress and strain, ore models dependent on damage.

6.1 Stress dependent failure criteria

One of the most simple models to predict failure is to consider that failure occures when the stress reaches a critical value. Below follows a short review of some of the basic stress dependent failure criteria. All the models presented are isotropic, i.e. they have the same property in all directions of the material.

6.1.1 Maximum principle stress criterion

The maximum principle stress criterion is also known as the Coulomb or Rankine failure criterion. It only depends on the principle stress to predict failure. To predict failure one considers two material parameters describing the maximum allowed stress in compression σ_c and tension σ_t , respectively, and state that failure is not to be expected as long as the principle stresses is in between these values, i.e.

$$-\sigma_c \leq \{\sigma_1, \sigma_2, \sigma_3\} \leq \sigma_t \quad (26)$$

This criterion can be visualized by a cube in the principal stress space and failure is not expected as long as the principal stress state is inside the cube. In a plane stress case, i.e $\sigma_3 = 0$, the allowed area is the shaded one shown in Figure 6.

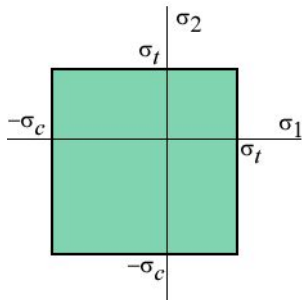


Figure 6: *Maximum principle stress in a plan stress case. Failure is not expected as long as the stress is inside the box*

6.1.2 Tresca's and von Mises' failure criteria

The two well known yielding functions by Tresca and von Mises, respectively describe when yielding occurs. The failure criteria is similar but instead of saying that yielding occurs when the functions value reaches the yield strength one is looking at the failure parameter σ_F . The simplest is the Tresca's criterion, which says that failure is not expected as long as the maximum differences between the principle stresses is lower then the fracture stress σ_F .

$$\sigma_F \geq \max(|\sigma_1 - \sigma_2|, |\sigma_2 - \sigma_3|, |\sigma_1 - \sigma_3|) \quad (27)$$

The von Mises' fracture criterion is given by

$$\sigma_F \geq \sqrt{\frac{1}{2}[(\sigma_1 - \sigma_2)^2 + (\sigma_2 - \sigma_3)^2 + (\sigma_3 - \sigma_1)^2]} \quad (28)$$

where σ_1, σ_2 and σ_3 are the principle stresses. For a tree-dimensional case the allowed volume is shown in Figure 7, where the von Mises' criterion becomes a cylinder which has its centerline along the hydrostatic axes $\sigma_1 = \sigma_2 = \sigma_3$. The Tresca's criterion is a hexagonal tube inside the cylinder. Failure is not expected as long as the principal stress state is inside the volumes. One drawback with these failure criteria is that they are not sensitive to hydrostatic stresses.

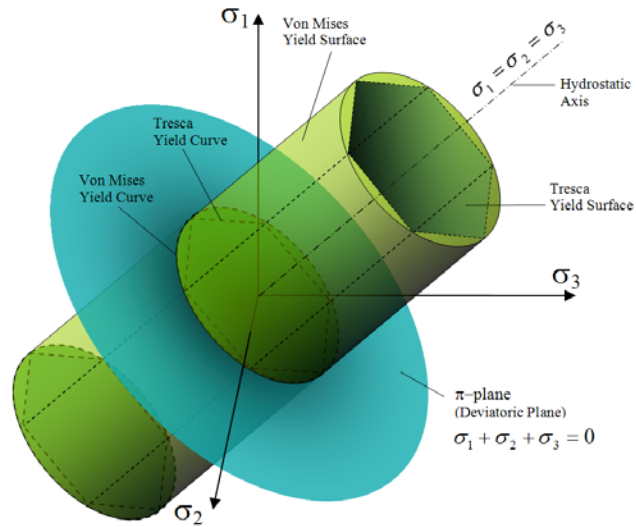


Figure 7: Yield surface according to Tresca and von Mises. From [11]

If a plan stress ($\sigma_3 = 0$) case is studied the Tresca's failure criterion becomes a hexagon and the von Mises' an ellipse that surrounds the hexagon in the stress plane, see Figure 8. As long as the stress is inside these surfaces no failure is expected.

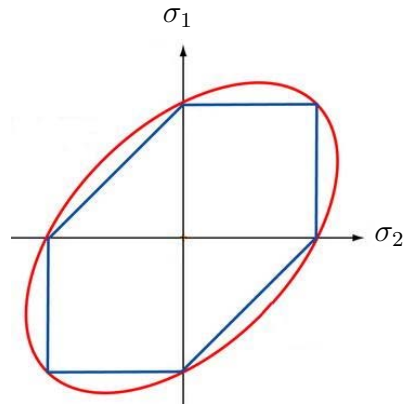


Figure 8: Tresca's and von Mises' failure criteria for a plane stress case. If the principle stresses are inside the area no failure is expected

6.1.3 Mohr's failure criterion

Mohr's failure criterion is also known as the Coulomb-Mohr failure criterion or the internal-friction theory. It is based on Mohr's circle and includes, just like the maximum principle stress criterion, only two material parameters, σ_c and σ_t . But in this case one also considers the shear stresses in order to predict failure. In this model one constructs two circles in a diagram showing shear stress on the y-axis and normal stress on the x-axis. The first circle has the radius $(\frac{\sigma_c}{2})$ and a centre point in $(\frac{\sigma_c}{2}, 0)$, the second has the radius of $(\frac{\sigma_t}{2})$ and a centre point in $(-\frac{\sigma_t}{2}, 0)$. The circles are then connected to each other with lines according to Figure 9. Failure is not expected as long as the Mohr's circles of the actual stress state can be constructed inside this area. In Figure 9 the Mohr circles are drawn in dashed lines for a case when no failure is expected.

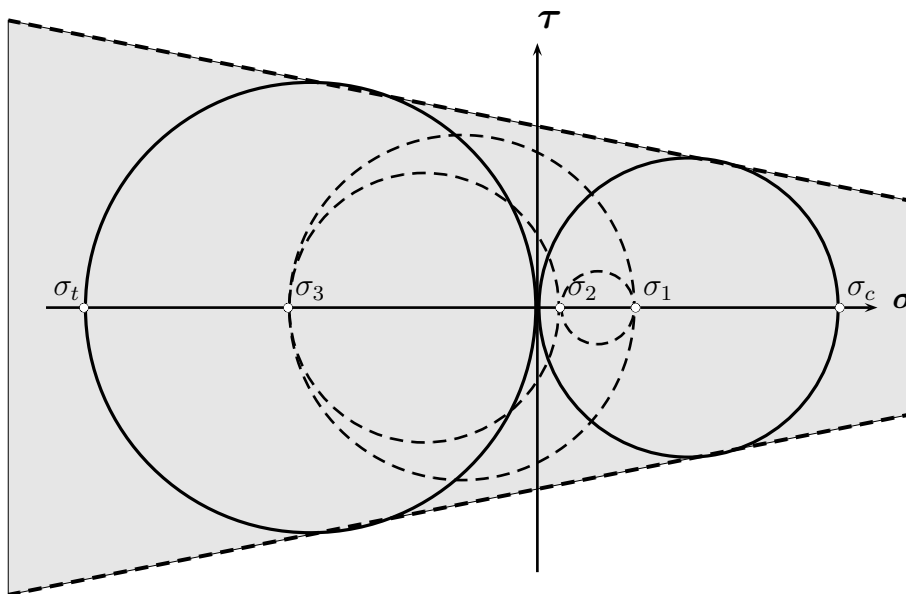


Figure 9: *Mohr's failure criterion. Failure is not expected as long as the Mohr circles are inside the dashed lines*

6.2 Strain dependent failure criteria

Other simple failure criteria consider the strains to fracture. Below follows a short review of some of the basic strain dependent failure criteria.

6.2.1 Maximum principle strain criterion

This may be one of the most simple failure criterion and it implies that failure is not expected as long as the maximum principle strain value is lower than a critical value ε_f , which is considered as a material parameter, i.e.

$$\{\varepsilon_1, \varepsilon_2, \varepsilon_3\} \leq \varepsilon_f \quad (29)$$

where $\varepsilon_1 \dots \varepsilon_3$ are the principal strains.

6.2.2 Constant equivalent strains criterion

Another basic failure criterion is to state that failure will occur when the equivalent strain $\bar{\varepsilon}$ reaches a critical value $\bar{\varepsilon}_f$.

$$\bar{\varepsilon} \leq \bar{\varepsilon}_f \quad (30)$$

For an incompressible plastic material obeying the von Mises' equivalent stress, the equivalent strain is defined as

$$\bar{\varepsilon} = \sqrt{\frac{2}{3} (\varepsilon_1^2 + \varepsilon_2^2 + \varepsilon_3^2)} \quad (31)$$

where $\varepsilon_1 \dots \varepsilon_3$ are the principal strains.

6.2.3 Forming Limit Diagram

The forming limit diagram (FLD) is often used in the analyses of forming processes to determine how close the material is to failure. The FLD was first developed by Keeler-Backhofen and Goodwin in the 60's, c.f. Stoughton and Zhu [12]. The main part of the FLD is the experimental construction of the forming limit curve (FLC) which can be represented in a diagram with the first and second principle strains as axes, see Figure 10. One drawback with the FLD is that it is only valid when the loading path is proportional, i.e. the ratio of the plastic strains must be constant throughout the forming process. This means that one needs to have a new FLC if any pre-strain or if any nonlinear loading path is used. It is also possible to present other failure criteria in the FLD like what has been done in the report by Eriksson et al. [13]. In this report the Cockcroft and Latham and the Bressan and Williams failure criteria are represented, and the benefit by showing all in the same FLD is that it is possible to see which failure criterion causes the failure.

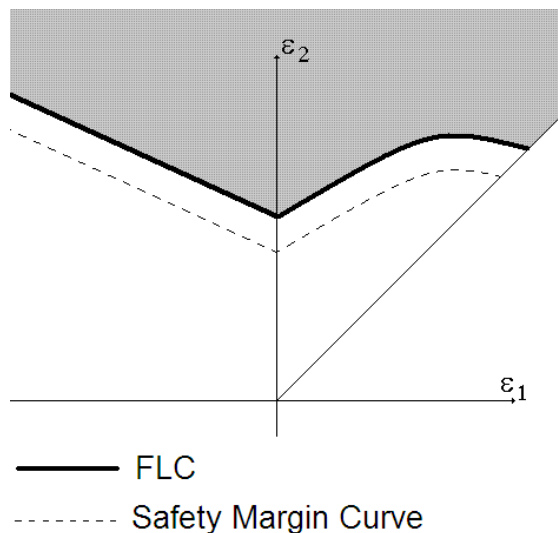


Figure 10: *Forming Limiting Diagram*

6.3 Cockcroft-Latham

Cockcroft and Latham [14] suggested that a criterion based on both stresses and strains might be beneficial. More precisely they argued that the plastic work must be an important factor. The total amount of plastic work done per unit volume at the fracture point can be formed from

$$\int_0^{\varepsilon_f} \sigma d\varepsilon_p \quad (32)$$

where $\sigma = \sigma(\varepsilon)$ is the current stress and ε_f is the fracture strain. However, the current stress σ unlike the peak stress σ_1 , is not influenced by the shape of the necked region. A criterion based on the total amount of plastic work therefore states that the shape of the neck should not have effect of the fracture strain, which is contrary to experiments. Therefore, the total amount of plastic work can not provide a good criterion by itself as the neck play an imported role according to experiments.

A more reasonable criterion of ductile fracture would be to take the magnitude of the highest normal stress into account. Therefore, it is proposed that fracture occurs in a ductile material when the quantity

$$\int_0^{\varepsilon_f} \bar{\sigma} \left(\frac{\sigma_1}{\bar{\sigma}} \right) d\bar{\varepsilon}_p \quad (33)$$

reaches a critical value for a given temperature and strain rate. Furthermore, $\bar{\sigma}$ is the equivalent stress, ε_f the strain at fracture, $\bar{\varepsilon}_p$ the equivalent plastic strain and $\left(\frac{\sigma_1}{\bar{\sigma}} \right)$ a non-dimensional stress concentration factor representing the effect of the highest tensile stress, σ_1 . The reduced form

$$\int_0^{\varepsilon_f} \sigma_1 d\bar{\varepsilon}_p \quad (34)$$

is used for the evaluations, and this integral reaches a critical value C at failure where C is a material constant. If all the principal stresses are smaller or equal to zero no fracture will occur according to this model. This model implies that failure in a ductile material depends both on stresses and plastic strains, i.e. neither stress nor strain alone can describe ductile fracture. Later modifications of the Cockcroft and Latham model have been made by Brozzo et al., Clift et al. and Oyane et al., see Heung and Keun-Hwan [15].

6.4 Shear instability

Plastic deformation is caused by slip on certain preferred slip systems, i.e. combinations of closed-packed crystallographic planes and directions. To make it possible to get plastic deformation, the shear stress needs to exceed a certain critical value τ_c that depends on the material.

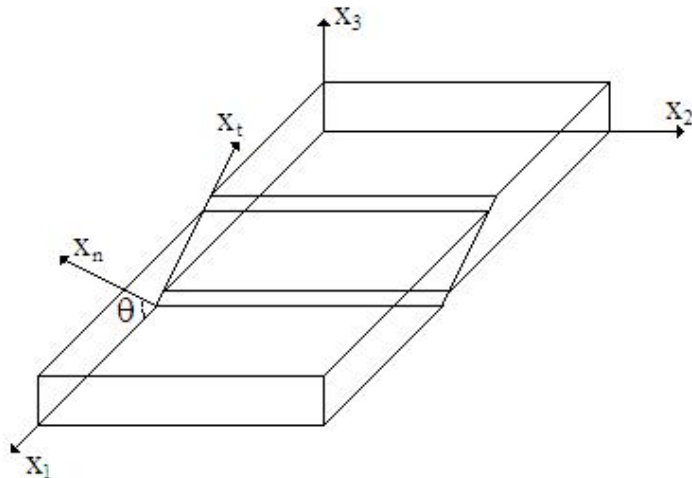


Figure 11: *Local necking of thin metals*

In Bressan and Williams [16] the authors suggest a shear instability criterion that says that the plastic strain in x_t -direction, see Figure 11 should be equal to zero. Due to the transformation of a second order tensor, the strain in the x_t -direction expressed in the main strain components becomes

$$d\varepsilon_t^p = \sin^2 \theta d\varepsilon_1^p + \cos^2 \theta d\varepsilon_3^p = 0 \quad (35)$$

This expression can be rewritten as

$$\cos 2\theta = \frac{d\varepsilon_1^p + d\varepsilon_3^p}{d\varepsilon_1^p - d\varepsilon_3^p} \quad (36)$$

if the plastic volume is constant, i.e. $d\varepsilon_1^p + d\varepsilon_2^p + d\varepsilon_3^p = 0$, and with $\beta = \frac{d\varepsilon_2^p}{d\varepsilon_1^p}$, this expression becomes

$$\cos 2\theta = -\frac{\beta}{2 + \beta} \quad (37)$$

If the same rotation, as for the strain, is done in the Mohr circle for the stresses, see Figure 12, the following equation is obtained

$$\sin 2\theta = \frac{\tau_c}{\frac{\sigma_1}{2}} \quad (38)$$

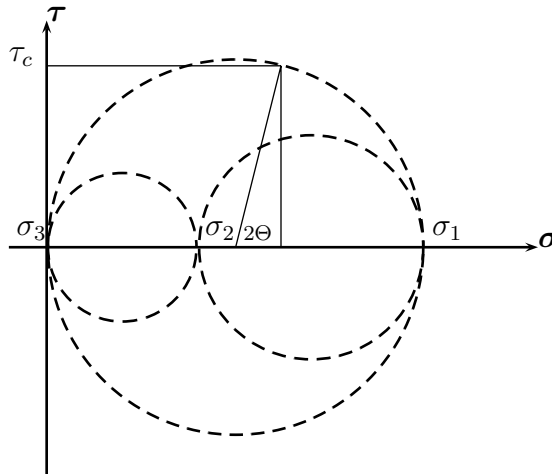


Figure 12: *Mohr's circle*

By using Equations (37) and (38) one finally obtains

$$\sigma_1 = \frac{2\tau_c}{\sqrt{1 - \left(\frac{\beta}{2+\beta}\right)^2}} \quad (39)$$

where σ_1 is the largest principle stress, τ_c is the critical shear stress, which is determined by experiments, and β , as shown above, is a relationship between the strains in the plane.

6.5 Damage models

In recent years models concerning different types of damage have been studied. In all these models some damage parameter has been considered. The damage parameter explains how much of the material that is damaged. One simple way to consider this damage is proposed by Lemaitre and Chaboche [7], i.e. as a relationship between the initial area and the damaged area in a certain direction

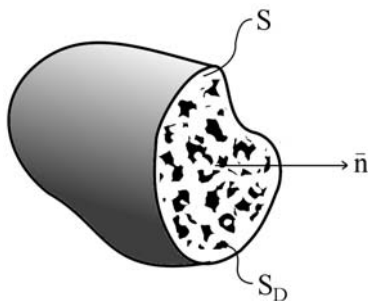


Figure 13: *Definition of the damage parameter*

$$D_n = \frac{S_D}{S} \quad (40)$$

where D_n is the damage variable, S_D and S are the damaged area and the initial area in the \vec{n} direction, respectively, see Figure 13. In this definition of damage ultimate failure is expected when D_n reaches the value of 1, i.e. when the whole surface is damage and there is no material left to hold the parts together. The area that can hold the load in the material is the difference between the damaged and the initial area ($S - S_D$) and if one considers the stress far away from the damaged region (σ_∞) and evaluate the effective stress working on the material in the damaged region, it could be calculated as

$$\sigma_{eff} = \frac{S\sigma_\infty}{S - S_D} = \frac{\sigma_\infty}{1 - D_n} \quad (41)$$

Many authors describe the benefits and the selection of material parameters for models concerning damage variables, e.g Feucht et al. [9], Ockewitz and Sun [17] and Poizat et al. [18].

6.5.1 Gurson

The original Gurson model [19] considers a damage parameter that describes the porosity f of the material. The damage parameter can vary from a value f_0 for undamaged material, to $f = 1$ for a completely damaged material. Because of the inability of predicting instability caused by coalescence of microvoids the Gurson model was modified by Tvergaard and Needleman [20]. The model is using the yield condition

$$\Phi = \frac{\sigma_{vM}^2}{\sigma_Y^2} + 2q_1 f^* \cosh\left(\frac{\text{tr}\boldsymbol{\sigma}}{2\sigma_Y}\right) - 1 - (q_1 f^*)^2 = 0 \quad (42)$$

where $\boldsymbol{\sigma}$ is the macroscopic stress tensor, σ_{vM} the von Mises equivalent stress, σ_Y the actual yield stress of the matrix material, q_1 is a constant that amplifies the hydrostatic stress effect for all strain levels and f^* is the effective void volume fraction given by

$$f^*(f) = \begin{cases} f & \text{if } f \leq f_c \\ f_c + \frac{1/q_1 - f_c}{f_f - f_c}(f - f_c) & \text{if } f > f_c \end{cases} \quad (43)$$

where f is the void volume fraction, f_c the critical void volume fraction, and f_f is the void volume fraction at rupture. The above equations explain the behaviour for a material when a specific void volume is considered. However, when a material is subjected to higher strain levels, the void volume is increasing. There are two phenomena that contribute to the increase of void volume: the first one is the growth of voids and the second one is the origin (nucleation) of new voids. As a consequence, the increase in void volume is

$$\dot{f} = \dot{f}_{growth} + \dot{f}_{nucleation} \quad (44)$$

since the matrix material is plastically incompressible the growth of voids can be expressed as

$$\dot{f}_{growth} = (1 - f)\text{tr}\dot{\boldsymbol{\epsilon}}^p \quad (45)$$

where $\dot{\boldsymbol{\epsilon}}^p$ is the rate of plastic strain. The nucleation is a phenomenon resulting from the stress level, strain level or a combination of these. Therefore, its definition needs substantial experimental support because it depends

heavily on the material that is being studied. One of the most studied cases corresponds to the situation when the nucleation is produced by plastic strain and is given by

$$\dot{f}_{nucleation} = A\dot{\varepsilon}_{eq}^p \quad (46)$$

where $\dot{\varepsilon}_{eq}^p$ is the equivalent plastic strain rate and A is the cavity nucleation rate given by

$$A = \frac{f_n}{s_N \sqrt{2\pi}} e^{-1/2 \left(\frac{\varepsilon_{eq}^p - \varepsilon_N}{s_N} \right)^2} \quad (47)$$

where f_n is the volume fraction of void nucleating particles, ε_N is the mean strain for nucleation and s_N is the standard deviation. The Gurson model strongly depending on the element size and to eliminate this effect it is possible to make the parameters f_f , f_c and f_n dependent on the element size l_e , that is

$$f_f = f_f(l_e) \quad f_c = f_c(l_e) \quad f_n = f_n(l_e)$$

This topic is further discussed in the report by Feucht et al. [9]. More recent reports based on the Gurson model are presented by e.g. Springmann and Kuna [21] and Alegre and Gutiérrez-Solana [22].

6.5.2 Johnson-Cook

The Johnson-Cook failure model [23] and [24] is a purely phenomenological model and is based on the plastic strain. The model use a damage parameter D and when this parameter reaches the value of 1, ultimate fracture is expected. The definition of the damage parameter is

$$D = \int \frac{1}{\varepsilon_f} d\varepsilon_{eq}^p \quad (48)$$

where ε_f is the equivalent strain to fracture and $d\varepsilon_{eq}^p$ is the increment of equivalent plastic strain. The expression for the equivalent strain to fracture is given by

$$\varepsilon_f = \left(d_1 + d_2 e^{-d_3 \frac{\sigma_m}{\sigma_{vM}}} \right) \left[1 + d_4 \ln \left(\frac{\dot{\varepsilon}_{eq}^p}{\dot{\varepsilon}_0} \right) \right] (1 + d_5 T) \quad (49)$$

where $d_1 \dots d_5$ are material constants, which can be determined from experiments. σ_m is the average of the three normal stresses, σ_{vM} is the von Mises equivalent stress, $\dot{\varepsilon}_{eq}^p$ is the rate of the von Mises plastic equivalent strain, $\dot{\varepsilon}_0$ is a reference strain rate and T is the corresponding temperature. As one can see in the Equations (48) and (49) the model depends on strain, strain rate, temperature and stress triaxiality, where the relationship $\left(\frac{\sigma_m}{\sigma_{vM}} \right)$ is a measure of the latter.

6.5.3 Wilkins

The model by Wilkins [25], also known as the $R_c D_c$ model, states that two factors increase the damage: the hydrostatic stress and the asymmetric stress. The hydrostatic stress accounts for the growth of holes by spalling. Interrupted tension tests have shown initiation and growth of voids that are forming a fracture surface. The asymmetric stress accounts for the observation that the elongation at failure decreases as the shear load increases in fracture tests with combined stress loads. The simplest expression for the damage D , which takes both the hydrostatic stress and asymmetric stress in to account, is

$$D = \int \omega_1 \omega_2 d\varepsilon_e^p \quad (50)$$

$$\omega_1 = \left(\frac{1}{1-\gamma\sigma_m} \right)^\alpha \quad \omega_2 = (2 - A_D)^\beta \quad (51)$$

$$A_D = \min \left(\left| \frac{s_2}{s_3} \right|, \left| \frac{s_2}{s_1} \right| \right) \quad (52)$$

where ω_1 is the hydrostatic pressure weight, ω_2 is the asymmetric stress weight, $d\varepsilon_e^p$ is the equivalent plastic strain increment, σ_m is the hydrostatic pressure, $s_1 \dots s_3$ is the principal stress deviators and α , β and γ are material constants. The parameter A_D ranges from 0 to 1 and when $A_D = 1$ the stress field is symmetric (and asymmetric when $A_D = 0$). The Wilkins model is expecting failure when D reaches a critical value D_C

$$D_c = D_0 (1 + b |\nabla D|^\lambda) \quad (53)$$

where ∇D is the damage gradient and D_0 , b and λ are material parameters. Due to its non-local form, Equation (53) is less mesh dependent than, e.g., the Johnson-Cook model.

7 Plane strain test sample

As an example a plane strain test is analysed with material model "Strong texture material" MAT_135, in LS-DYNA, Hallqvist [26] and Hallqvist [27]. The material model MAT_135 has three different failure criteria, first there is a critical thickness strain (CTS), which implies that if the plastic strain in the thickness direction reach a critical value the element is considered as failed and is deleted. The material model also contains the Cockcroft-Latham (C-L) and the Bressan-Williams (B-W) criteria, which previously have been discussed. The test is to be done assuming the Duplex steel DP800 and the material parameters, taken from Eriksson [13], are presented in Tables 1 and 2. The values of the parameters for C-L and B-W are taken from the same report, the C-L parameter is set to $C = 530$ MPa and the B-W is set to $\tau_c = 590$ MPa. The critical thickness strain parameter ε_{tc} is calculated from the fact that the plastic elongation on a specimen that is $L_0 = 80$ mm elongates 10 % before fracture, i.e. $A_{80} = 0.1$, from [28]. With this value the total elongation before fracture is calculated as

$$A_{80} = \ln \frac{L_f}{L_0} \Rightarrow L_f = L_0 e^{A_{80}} = 80 e^{0.1} \approx 88.41 \text{ mm} \quad (54)$$

However it is assumed that the plastic strains appears on a local necked region whith a length of the same size as the thickness. Thus the total elongation of $L_f - L_0 = 8.41$ mm takes place on a distance that is $\hat{L}_0 = 1.5$ mm. Which means that

$$\varepsilon_{Lc} = \ln \frac{L_f - L_0 + \hat{L}_0}{\hat{L}_0} = \ln \frac{9.91}{1.5} \approx 1.89 \quad (55)$$

Then the plastic strain in the length direction is known. From plastic volume constance, one fine

$$\varepsilon_L + \varepsilon_w + \varepsilon_t = 0 \quad (56)$$

where ε_L , ε_w and ε_t is the plastic strain in length, width and thickness directions.

The relationship between the strain in the thickness and width direction can be given by the value $R_0 \approx \frac{\varepsilon_w}{\varepsilon_t}$ and is given in Table 2. Equation (56) can then be written.

$$\varepsilon_L + (1 + R_0)\varepsilon_t = 0 \Rightarrow \varepsilon_{tc} = -\frac{\varepsilon_{Lc}}{1+R_0} = -\frac{0.98}{1+0.75} = -1.08 \quad (57)$$

Thus, in the simulations the critical thickness strain is set to $\varepsilon_{tc} = -1.08$.

Table 1: *The extended Voce strain hardening parameters*

Parameter	σ_Y [MPa]	Q_{R1} [MPa]	C_{R1}	Q_{R2} [MPa]	C_{R3}
Value	392	201	51	362	5.23

Table 2: *Dimensionless anisotropy coefficients from uniaxial loading tests*

Material	$(\sigma_0/\sigma_0)_{avg}$	$(\sigma_{45}/\sigma_0)_{avg}$	$(\sigma_{90}/\sigma_0)_{avg}$	R_0	R_{45}	R_{90}
DP800	1.00	1.00	1.00	0.75	1.01	1.06

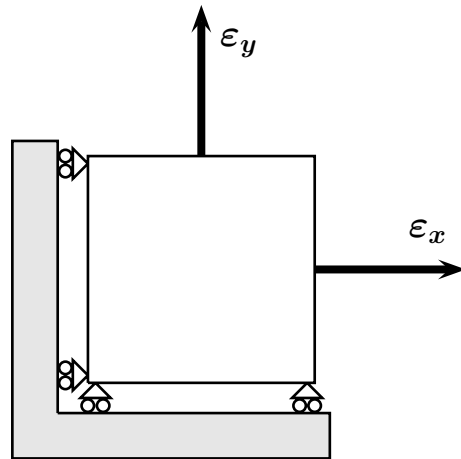


Figure 14: *One element.*

First simulations is carried out for only one element which is given a prescribed elongation, see Figure 14. The relation between the strain in the x- and y-direction is constant for different load cases according to

$$\varepsilon_x = \alpha\varepsilon_y \tag{58}$$

where for a plane strain case the constant α is equal to 0. The simulation is then carried out for three different failure criteria, C-L, B-W and CTS. However, the extended Voce hardening has one drawback, i.e. the stress converges towards a final value. The values of the Voce parameters according to Table 1 give a converges towards 955 MPa, which means that the B-W failure model never fails for a plane strain case, i.e. $\sigma_1 \leq 2\tau_c$. In the work by Eriksson [13] an improved hardening parameter is included, i.e. the hardening is first given by the Voce law but when the slope of the curve is below a critical value the hardening is set to continue in this direction. The value of this slope is first set to $\sigma_{100} = 1250$ MPa, in agreement with Eriksson, then the value is changed to 802 MPa, which is the slope of the curve at local necking. The result indicates that the Bressan-William failure criterion is more dependent of a correct hardening than the Cockcroft-Latham criterion, see Figures 15 and 16.

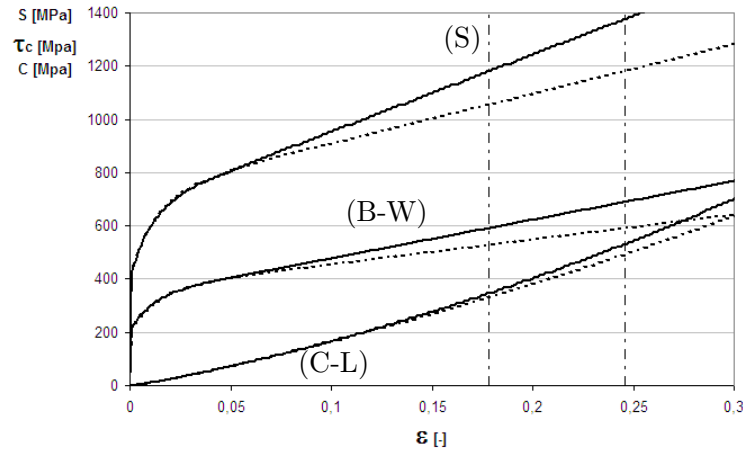


Figure 15: Growth of the Bressan-Williams and the Cockcroft-Latham failure parameters as a function of the strain for a plane strain case. The upper curve marked S is the stress curve for the material. Two different type of hardening are used, 802 MPa (dashed) and 1250 MPa (solid)

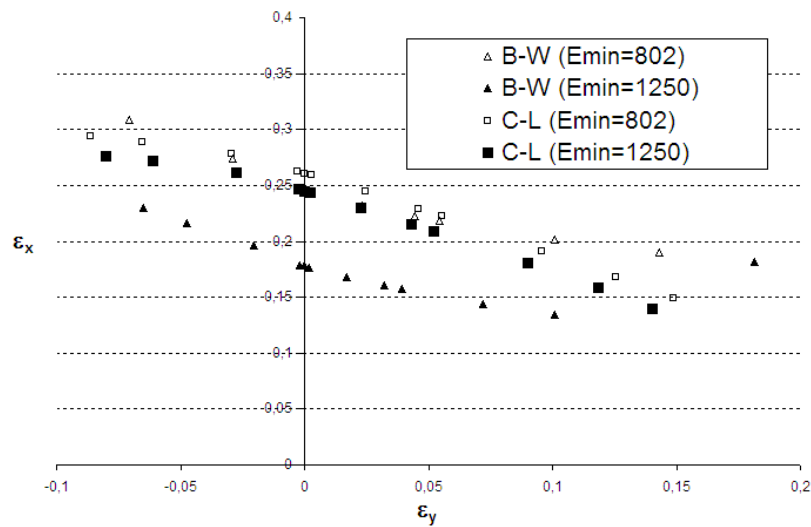


Figure 16: Bressan-Williams and the Cockcroft-Latham failure for different strain path

After the first simulation with only one element a plane strain specimen, with geometry according to the one used by Eriksson, see Figure 17, is carried out.

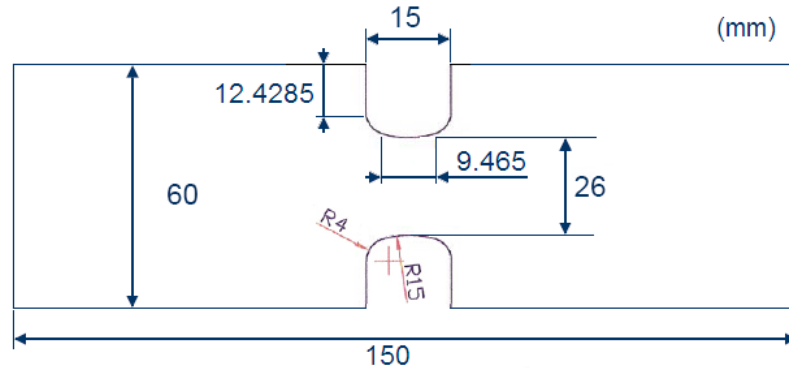


Figure 17: *Specimen geometry*

Five different types of simulations have been carried out with different failure models active: the first one with a failure criterion according to C-L, the second one according to B-W, the third one according to CTS, the fourth one assuming a combination of the C-L and the B-W criteria and the final one assuming a combination of all three failure criteria.

As boundary condition one node on the left edge has been fixed in all directions while the other nodes on the same side have been fixed in the length direction. On the other side all nodes are given a smoothly increasing translation in the length direction realized by the LS_DYNA keyword DEFINE_CURVE_SMOOTH. For all simulations the improved hardening parameter has been chosen to $\sigma_{100} = 1250$ MPa.

In the first simulation with the plane strain specimen, where only the C-L failure criterion is used, the failure is initiated at the edge and is growing towards the middle of the specimen, see Figure 18. The total displacement of the right edge at the final fracture is $u \approx 5.9$ mm. Even in the second simulation, when only B-W failure criterion is used, the failure is initiated at the edges and is growing towards the middle of the specimen, see Figure 19. However, in this case the total displacement at final fracture is shorter $u \approx 5.2$ mm. The third simulation with the CTS criterion, predicts that the failure is initiated in the middle and is growing towards the edges, see

Figure 20. The total displacement at fracture for this case is $u \approx 9.8 \text{ mm}$. The remaining simulations with combinations of the different failure criteria show that different elements can fail due to different criteria, see Figures 21 and 22, the displacement for the final cases is $u \approx 5.2 \text{ mm}$. According to the tests performed by Eriksson the displacement at fracture should be lower. However, if a different second hardening value is used the total displacement at fracture can be reduced significantly. For instance when a hardening parameter of 802 MPa is used the displacement at fracture is $u \approx 3 \text{ mm}$ according to the simulation. The larger displacement is caused by the bigger plastic zone that arise in the model when a faster hardening is used. It can also be argued that the element size plays an important role.

When a real test is studied, see Figure 23, it is seen that the fracture surface looks quite similar to the one obtained by a simulation based on a combination of all failure criteria. It seems that different elements are failing due to different criteria.

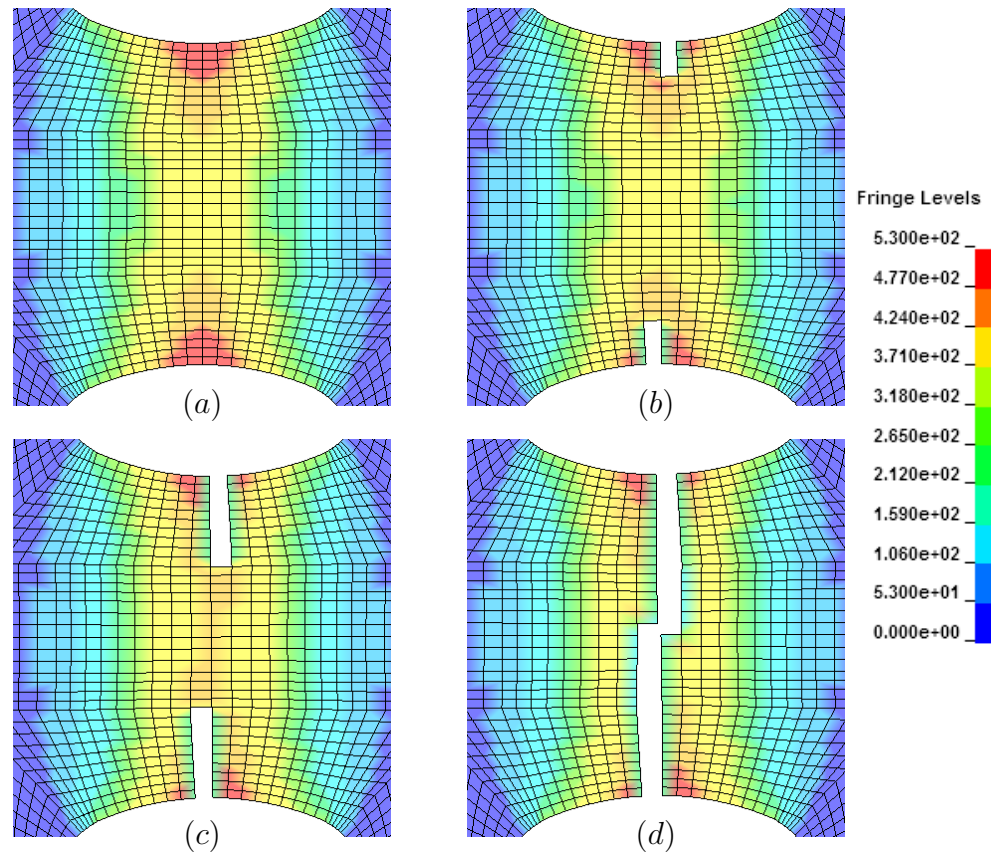


Figure 18: *Plane strain failure test with Cockcroft-Lathams failure criterion (a) before failure starts, (b) failure is initiated at the edges, (c) the failure is growing towards the mid point, (d) final failure. The fringe levels show the values of the Cockcroft-Latham failure parameter*

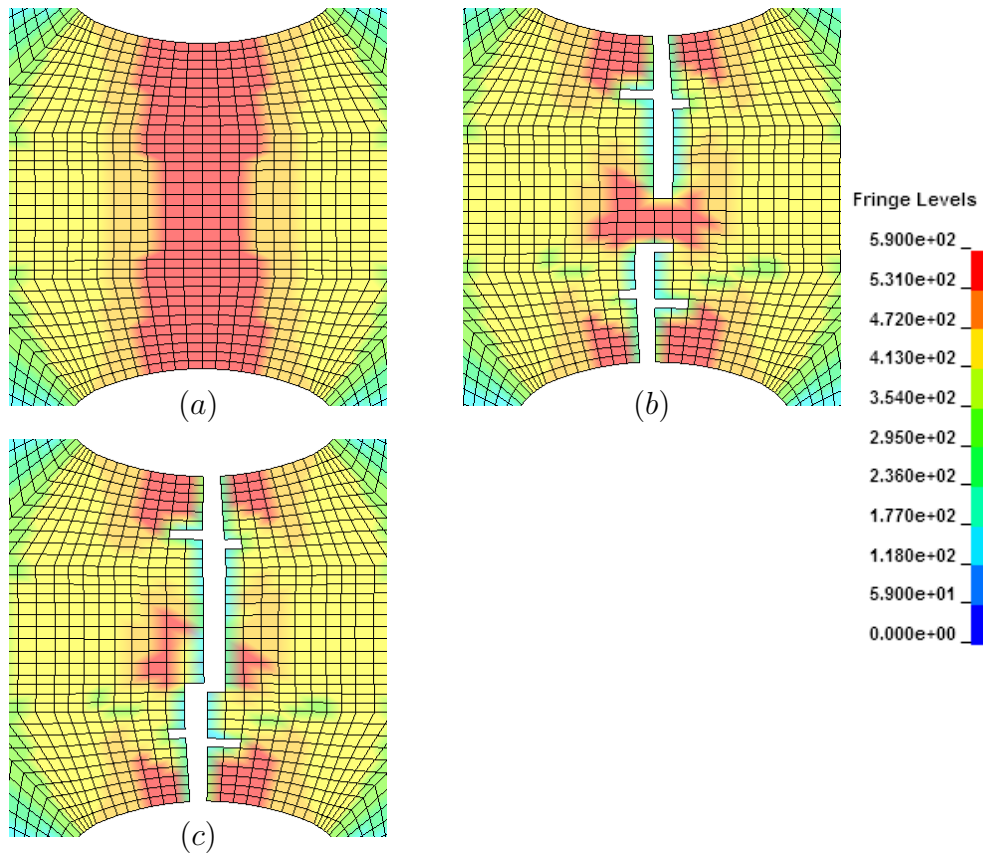


Figure 19: *Plane strain failure test with Bressan-Williams failure criterion (a) before failure starts, (b) failure is initiated at the edges, (c) final failure. The fringe levels show the values of the Bressan-Williams failure parameter*

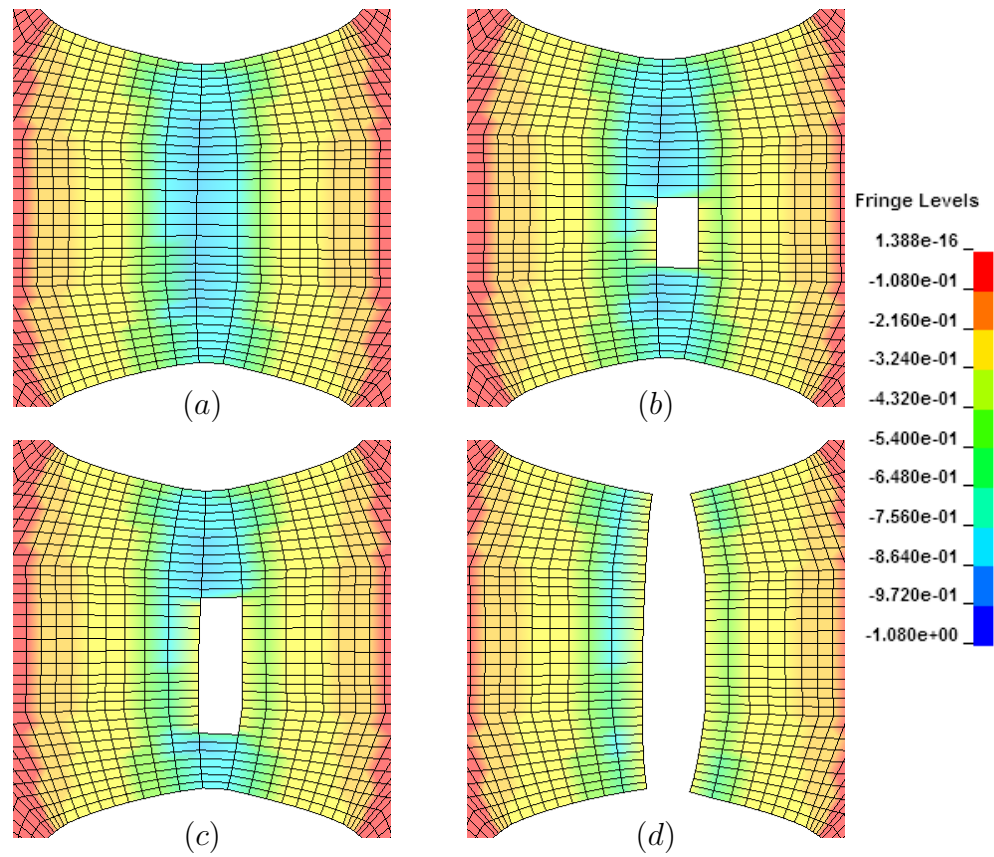


Figure 20: *Plane strain failure test with critical thickness strain failure criterion (a) before failure starts, (b) failure is initiated in the center of the specimen, (c) failure propagating, (d) final failure. The fringe levels show the values of the strain in the thickness direction*

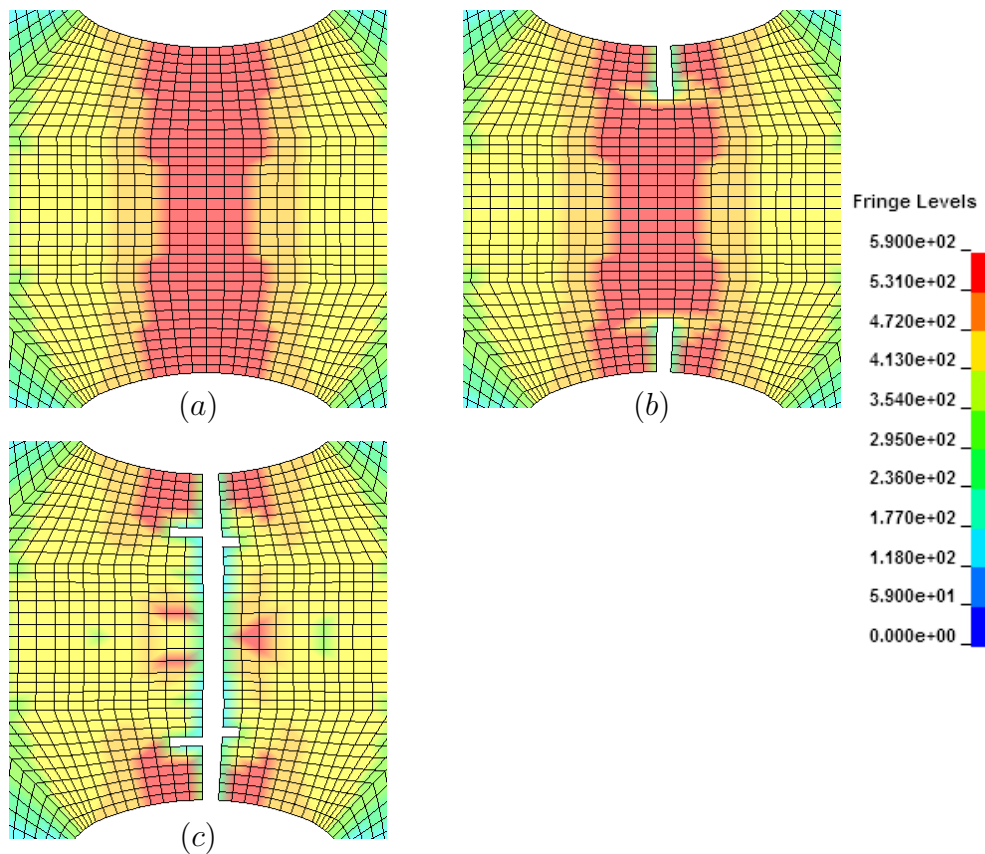


Figure 21: *Plane strain failure test with, Cockcroft-Latham and Bressan-Williams failure criteria (a) before failure starts, (b) failure is initiated at the edges, (c) final failure. The fringe levels show the values of the Bressan-Williams failure parameter*

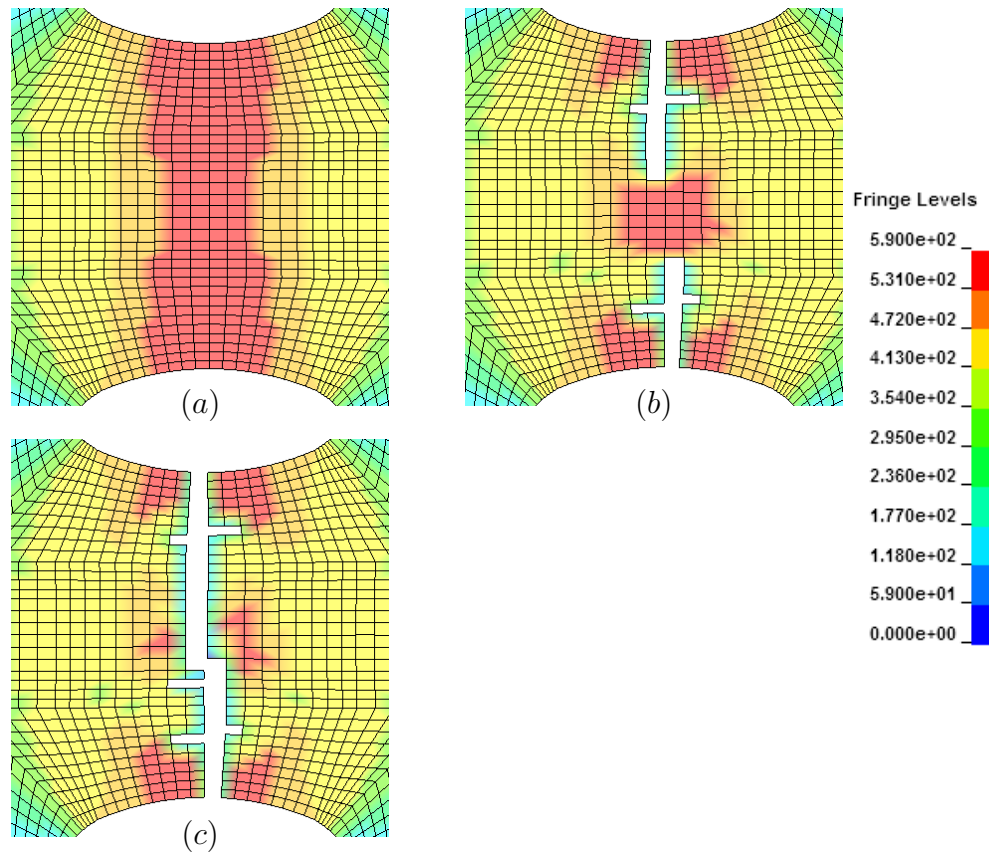


Figure 22: *Plane strain failure test with Cockcroft-Latham, Bressan-Williams and critical thickness strain failure criteria (a) before failure starts, (b) failure is initiated at the edges, (c) final failure. The fringe levels show the values of the Bressan-Williams failure parameter*



Figure 23: *Real plane strain failure test of DP800. From [13]*

8 Conclusions and discussion

One of the main reasons for the poor agreement between simulations and real tests, when using the simple failure models only considering stresses or strains, is the element size dependency. If an element is failing in a simulation it causes a concentration of the stress in the neighbouring elements which might fail immediately. Therefore, if a failure is started in an element a chain reaction is causing a complete failure of the specimen. A model that does not regard what happens in the neighbouring elements is called local, and the opposite is a non-local model. The model of Wilkins is a non-local model as the damage gradient concerns the behaviour of the neighbouring elements.

One of the main drawbacks of the more advanced phenomenological failure models are the many material parameters, that have to be determined from material tests. Another drawback is, as mentioned earlier, that they are quite element size dependent and sometimes the material parameters have to be set for a specific element size, e.g. using the Gurson model.

Another problem, when considering failure in components, is to take care of what has happened before, i.e. if the component has any internal faults like micro-voids or crazing that have arisen during the creation of the material. It is also interesting to consider how the material has been formed, i.e. to what extent it has undergone plastic deformations. It is thus often necessary to modify the material description in order to take into account its history. As an example in the case when a damage model is used, e.g. Gurson, Johnson-Cook or Wilkins, it is not necessary that the damage parameter starts from zero. Even in some of the other models the parameter describing damage can be set to an initial value to describe a previous deformation history.

As could be seen in the previous section, it is for a plane strain test not sufficient with only one failure criterion, as adopted in the first part of the experiment, see Figures 18, 19 and 20. When comparing this to the actual fracture surface of the plane strain specimen, see Figure 23, it is obvious that it does not correspond well to experiment. However, when the simulation is based on a combination of the failure criteria the agreement is improved c.f. Figure 22. It is thereby clear that it might be a combination of different failure models that is causing the failure of the elements. As shown in the previous section it is also important to have a good material model that correctly describes the hardening of the material.

References

- [1] Mase G. T., Mase G. E., (1999), *Continuum Mechanics for Engineers*. Boca Raton: CRC Press.
- [2] Spencer A. J. M., (1980), *Continuum Mechanics*. New York: Dover Publications.
- [3] Belytschko T., (2000), *Nonlinear Finite Elements for Continua and Structures*. Chichester: John Wiley.
- [4] Askeland D. R., (1984), *The Science and Engineering of Materials*. Sheffield: Nelson Thorens Ltd.
- [5] Hertzberg R.W., (1996), *Deformation and Fracture Mechanics of Engineering Materials*. Hoboken: John Wiley.
- [6] Dieter G. E., (1986), *Mechanical Metallurgy*. McGraw-Hill.
- [7] Lemaitre J., Chaboche J.-L., (1990), *Mechanics of Solid Materials*. Cambridge: Cambridge University Press.
- [8] Dahlberg T., Ekberg A., (2006), *Failure Fracture Fatigue*. Lund: Studentlitteratur.
- [9] Feucht M., Sun D.-Z., Erhart T., Frank T., (2006), Recent Development and Applications of the Gurson Model, *LS-DYNA Anwenderforum, Ulm*, 2006.
- [10] Wierzbicki T., Bao Y., Lee Y.-W., Bai Y., (2005), Calibration and evaluation of seven fracture models. *International Journal of Mechanical Sciences* 47 pp. 719-743.
- [11] http://en.wikipedia.org/wiki/Image:Yield_surfaces.png (2008-02-28)
- [12] Stoughton T. B., Zhu X., (2004), Review of theoretical models of strain-based FLD and their relevance to the stress-based. *International Journal of Plasticity* 20 pp. 1463-1486.
- [13] Eriksson M., Lademo O.-G., Hopperstad O. S., Langseth M., (2007), *Deterministic material modelling for forming and crash analyses of metal components*. SINTEF, Materials and Chemistry, Trondheim. 85 pp.

-
- [14] Cockcroft M. G., Latham D. J., (1968), Ductility and the workability of metals. *Journal of the institute of metals* 96 pp, 33-39
- [15] Heung N. H., Keun-Hwan K., (2003), A ductile fracture criterion in sheet metal forming process. *Journal of Materials Processing Technology* 142, pp. 231-238
- [16] Bressan J. D., Williams J. A., (1983), The use of a shear instability criterion to predict local necking in sheet metal deformation. *International Journal of Mechanical Sciences* 25, pp. 155-168
- [17] Ockewitz A., Dong-Zhi S., (2006), Damage modelling of automobile components of aluminium materials under crash loading. *LS-DYNA Anwenderforum, Ulm*, 2006.
- [18] Poizat C., Campagne L., Daridon L., Ahzi S., Husson C., Merle L., (2005), Modeling and simulation of thin sheet blanking using damage and rupture criteria. *International Journal of Forming Processes* 8 pp. 29-47.
- [19] Gurson A. L., (1977), Continuum theory of ductile rupture by void nucleation and growth: Part I– Yield criteria and flow rules for porous ductile media. *Journal of Engineering Materials and Technology* 99(1) pp. 2-15.
- [20] Needleman A., Tvergaard V., (1984), An analysis of ductile rupture in notched bars. *Journal of Mechanical Physics of Solids* 32 pp. 461-490.
- [21] Springmann M., Kuna M., (2005), Identification of material parameters of the Gurson-Tvergaard-Needleman model by combined experimental and numerical techniques. *Computational Materials Science* 32 pp. 544-552.
- [22] Alegre J.M., Gutiérrez-Solana F., (2004), A Gurson-Tvergaard based model to simulate fracture of aged duplex stainless steels. *Fatigue Fracture Engne Mater Struct* 27 pp. 1171-1182.
- [23] Johnson G. R., Cook W. H., (1985), Fracture characteristics of three metals subjected to various strains, strain rates, temperatures and pressures. *Engineering Fracture Mechanics* 21 pp. 31-48.
-

-
- [24] Johnson G. R., Cook W. H., (1983), A constitutive model and data for metals subjected to large strains, high strain rates and high temperatures. *Presented at the Seventh International Symposium on Ballistics*, Hague.
- [25] Wilkins M. L., Streit R. D., Reaugh J. E., (1980), *Cumulative-Strain-Damage Model of Ductile Fracture: Simulation and Prediction of Engineering Fracture Test*. University of California, Livermore. 70 pp.
- [26] Hallquist J.O., (2006), *LS-DYNA Theory Manual*. Livermore: Livermore Software Technology Corporation.
- [27] Hallquist J.O., (2007), *LS-DYNA Keyword User's Manual*. Livermore: Livermore Software Technology Corporation.
- [28] <http://www.ssabdirect.com/templates/SteelfactsSearchProduct.aspx?id=5787> (2008-03-06)